AGU PUBLICATIONS

Water Resources Research

RESEARCH ARTICLE

10.1002/2015WR017453

LPMLE3: A novel 1-D approach to study water flow in streambeds using heat as a tracer

U. Schneidewind[1,2,3], M. van Berkel[4,5], C. Anibas[6], G. Vandersteen[7], C. Schmidt[8], I. Joris[1], P. Seuntjens[1,2,9], O. Batelaan[10], and H. J. Zwart[3,11]

[1]Environmental Modeling Unit, VITO—Flemish Institute for Technological Research, Mol, Belgium, [2]Department of Soil Management, Ghent University, Ghent, Belgium, [3]Department of Engineering Geology and Hydrogeology, RWTH Aachen University, Aachen, Germany, [4]Department of Mechanical Engineering, Eindhoven University of Technology, Eindhoven, Netherlands, [5]FOM Institute DIFFER, Dutch Institute for Fundamental Energy Research, Eindhoven, Netherlands, [6]Department of Hydrology and Hydraulic Engineering, VUB, Brussels, Belgium, [7]Department of Fundamental Electricity and Instrumentation, VUB, Brussels, Belgium, [8]Department of Hydrogeology, Helmholtz-Centre for Environmental Research-UFZ, Leipzig, Germany, [9]Department of Bioscience Engineering, University of Antwerp, Antwerp, Belgium, [10]School of the Environment, Flinders University, Adelaide, Australia, [11]Department of Applied Mathematics, University of Twente, Enschede, Netherlands

Key Points:
- 1-D method for studying water flow in the streambed using heat as a tracer
- Method is applicable for layered streambeds and results can be used in further analyses to delineate nonvertical water flow
- Method provides parameter uncertainties and model quality information

Supporting Information:
- Supporting Information S1

Correspondence to:
U, Schneidewind,
schneidewind@lih.rwth-aachen.de

Citation:
Schneidewind, U., M. van Berkel, C. Anibas, G. Vandersteen, C. Schmidt, I. Joris, P. Seuntjens, O. Batelaan, and H. J. Zwart (2016), LPMLE3: A novel 1-D approach to study water flow in streambeds using heat as a tracer, *Water Resour. Res.*, *52*, 6596–6610, doi:10.1002/2015WR017453.

Received 24 APR 2015
Accepted 30 JUL 2016
Accepted article online 5 AUG 2016
Published online 26 AUG 2016

Abstract We introduce LPMLE3, a new 1-D approach to quantify vertical water flow components at streambeds using temperature data collected in different depths. LPMLE3 solves the partial differential equation for coupled water flow and heat transport in the frequency domain. Unlike other 1-D approaches it does not assume a semi-infinite halfspace with the location of the lower boundary condition approaching infinity. Instead, it uses local upper and lower boundary conditions. As such, the streambed can be divided into finite subdomains bound at the top and bottom by a temperature-time series. Information from a third temperature sensor within each subdomain is then used for parameter estimation. LPMLE3 applies a low order local polynomial to separate periodic and transient parts (including the noise contributions) of a temperature-time series and calculates the frequency response of each subdomain to a known temperature input at the streambed top. A maximum-likelihood estimator is used to estimate the vertical component of water flow, thermal diffusivity, and their uncertainties for each streambed subdomain and provides information regarding model quality. We tested the method on synthetic temperature data generated with the numerical model STRIVE and demonstrate how the vertical flow component can be quantified for field data collected in a Belgian stream. We show that by using the results in additional analyses, nonvertical flow components could be identified and by making certain assumptions they could be quantified for each subdomain. LPMLE3 performed well on both simulated and field data and can be considered a valuable addition to the existing 1-D methods.

1. Introduction

The quantification of water fluxes across streambeds has become an important aspect in the study of coupled groundwater-surface water systems. Quantitative information regarding these fluxes is essential in the study of the transport and fate of contaminants [*Conant*, 2004; *Dujardin et al.*, 2014] and nutrients [*Krause et al.*, 2009; *Bardini et al.*, 2013; *Bartsch et al.*, 2014] in the hyporheic zone (HZ), i.e., the transition zone between groundwater and surface water. Streambed fluxes also play an important role in river management and restoration [*Bukaveckas*, 2007; *Daniluk et al.*, 2013; *Käser et al.*, 2013]. Magnitude and direction of streambed fluxes depend on a combination of (i) the pressure gradient between the stream and the connected aquifer; (ii) streambed morphology and sediment properties; and (iii) sediment load and deposition patterns. These issues have been reviewed by *Buss et al.* [2009] and *Boano et al.* [2014], and have been discussed in detail in many of the references therein.

Water fluxes across streambeds can be measured in the field using seepage meters [*Rosenberry*, 2008; *Fritz et al.*, 2009]. Fluxes can also be quantified using measurements of hydraulic heads and vertical hydraulic gradients [*Krause et al.*, 2012; *Noorduijn et al.*, 2014] or by conducting tracer experiments [*Engelhardt et al.*, 2011; *Langston et al.*, 2013]. An important tracer that has received increased attention over the recent years

is heat. Temperature information has, for example, been used to map zones of groundwater-surface water interaction [*Alexander and Caissie*, 2003], to quantify exchange fluxes for a variety of stream environments [*Bianchin et al*., 2010; *Nützmann et al*., 2014; *Schmadel et al*., 2014] or during extreme hydrologic events [*Barlow and Coupe*, 2009; *Karan et al*., 2014], and to investigate the influence of in-stream structures on hyporheic heat transport [*Hester et al*., 2009; *Menichino and Hester*, 2014].

Temperature measurements conducted both at the top of a streambed and at some depth are often used to quantify vertical streambed fluxes by numerically or analytically solving for coupled water flow and heat transport as summarized by *Anderson* [2005] and *Rau et al*. [2014]. Several analytical 1-D models have been developed that allow for the determination of purely vertical fluxes from temperature-time series [*Hatch et al*., 2006; *Keery et al*., 2007; *McCallum et al*., 2012; *Luce et al*., 2013]. These models have now been integrated into software packages such as VFLUX [*Gordon et al*., 2012; *Irvine et al*., 2015a]. Common to all these analytical 1-D models is their use of information on amplitude attenuation and phase lag, which a temperature signal at a certain frequency experiences as it propagates through the streambed. In most cases, streambed thermal parameters, such as thermal diffusivity are known or estimated with low uncertainty. However, the works of *Luce et al*. [2013] and *McCallum et al*. [2012] have also demonstrated the theoretical possibility to estimate vertical fluxes without prior accurate knowledge of those streambed thermal parameters if both amplitude attenuation and phase lag can be determined with sufficient accuracy.

In contrast to these analytical solutions, *Wörman et al*. [2012] demonstrated how vertical flux and thermal diffusivity can be quantified in the frequency domain by applying spectral scaling factors. They also showed that with such frequency domain approaches one can easily use temperature-information at multiple frequencies (a frequency spectrum) simultaneously for flux calculations (this could be, e.g., the diel and annual cycles, periodic temperature changes caused by anthropogenic influences, etc.), as compared to the approaches implemented in VFLUX that use only information from one frequency at a time. With LPML, *Vandersteen et al*. [2015] introduced another frequency domain method that can be used to quantify vertical flux and thermal diffusivity. In addition, this LPML method is able to automatically separate a temperature signal into periodic, nonperiodic (transient), and noise parts, to calculate uncertainties on the parameter estimates and to provide information regarding model quality. As such, these frequency domain approaches seem to be more powerful and versatile and researchers have started to use them in combination with other time series data, e.g., on water quality in catchments [*Riml and Wörman*, 2015].

All these approaches determine flux and thermal diffusivity using pairs or arrays of vertically distributed temperature sensors. As such, the temperature signal of the top sensor is considered the upper boundary while the lower sensor(s) show(s) the response of the streambed in terms of temperature. The location of the lower boundary condition is approaching infinity. This is based on the assumption that the subsurface is a semi-infinite halfspace (see, e.g., equation (6a) in *Luce et al*. [2013]). In this way, the vertical flow component and thermal parameters are assumed constant in space over the entire halfspace [see, e.g., also *Keery et al*., 2007]. However, with the introduction of multisensor devices (i.e., containing more than two vertically distributed temperature sensors at one measurement device) such as the one presented in *Schmidt et al*. [2014] or FO-DTS, i.e., fiber-optic distributed temperature sensors) [*Selker et al*., 2006; *Vogt et al*., 2010], researchers are now capable of collecting streambed temperature data with high vertical and temporal resolution. First attempts have been made to use such data and the aforementioned analytical solutions implemented in the VFLUX software to calculate vertical profiles of streambed fluxes varying with depth [*Briggs et al*., 2012, 2013]. For that, the upper boundary was shifted gradually downward. Although this approach can provide reasonable flux estimates, using a solution based on a semi-infinite halfspace also introduces additional errors [*van Berkel et al*., 2014b].

In reality, the temperature at a certain point within the streambed is determined by streambed forming processes as well as the characteristics of water flow. Streambed-forming processes, such as erosion, colmation, or sedimentation vary in time and space and many streambeds typically have a heterogeneous sediment structure. Thus, magnitude and direction of water flux may vary considerably [e.g., *Schornberg et al*., 2010; *Vogt et al*., 2010; *Boano et al*., 2014]. Water flow through the streambed is induced mostly by differences in hydrostatic (due to a difference in elevation of the overlying water column) or hydrodynamic (bedform-induced, flow around in-stream features) pressure heads. Other drivers of water flow could be turbulence in the overlying water column, wave, or tidal effects (mostly in coastal streams or estuaries) or biological activities including plant growth, microbial activity, or the activity of benthic organisms (see the recent review

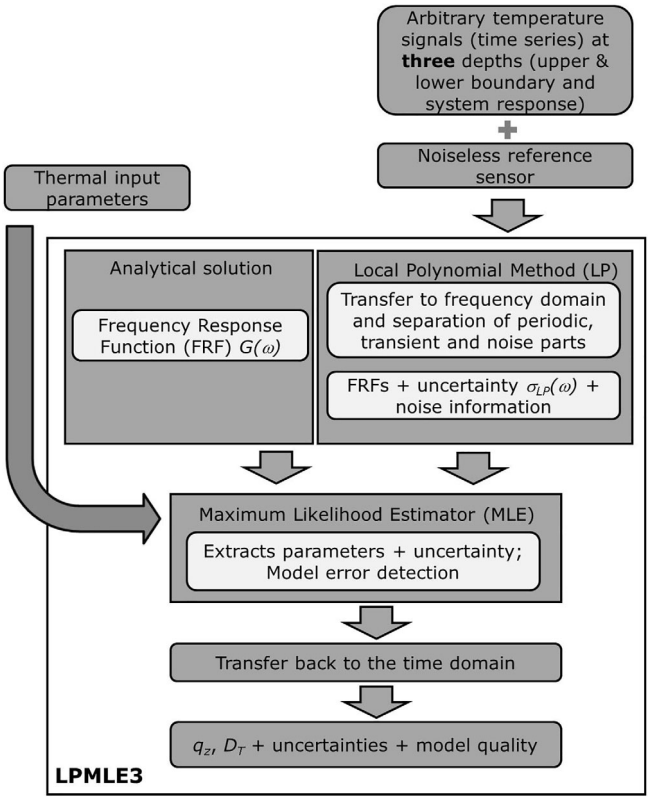

Figure 1. Flow chart presenting the concept of the LPMLE3 method.

paper of *Boano et al.* [2014 and references therein]). These processes define the mixing behavior of surface water and groundwater in the HZ and as such the nature of the flow field. Additionally, water could be stored in the streambed in a way similar to aquifer storage. However, due to the small volume streambeds or hyporheic zones typically encompass, storage may not play a significant role in most stream environments.

With this in mind the question can be raised regarding the validity or representativeness of vertical flux estimates in a three-dimensional flow field that can change its characteristics much faster in the HZ than in aquifers. Several studies discuss nonvertical flow components and their impact. For example, *Shanafield et al.* [2010] state that fully vertical flow can often only be encountered beneath the stream center, while closer to stream banks and with increasing distance from the streambed top, nonvertical flow components increase. *Lautz* [2010], *Roshan et al.* [2012], and *Cranswick et al.* [2014] used numerical models to study the performance of 1-D approaches in comparison with 2-D approaches where vertical and nonvertical flow components are present and found that assuming purely vertical flow can lead to considerable errors in flux estimates. In general, more work seems necessary to improve our understanding regarding nonvertical flow in the HZ and their impact on the validity of vertical flux estimates.

Here we introduce the *LPMLE3* method (Figure 1) that puts forward the idea of quantifying the vertical flow component and thermal diffusivity in the frequency domain using local boundary conditions. As such, the use of the semi-infinite halfspace concept, which is prone to errors, can be avoided. Vertical flow components can be quantified for finite streambed subdomains (or layers), which is more representative than assuming the streambed as homogeneous. Results were used in additional analyses to delineate nonvertical flow components. First, we present the mathematical theory behind the LPMLE3 method. Then, we test its applicability on a synthetic data set. Afterward, we quantify vertical flow components for finite streambed subdomains under field conditions using temperature data obtained from the Slootbeek, a small Belgian lowland stream and delineate horizontal flow components. Finally, we show a possibility how the magnitude of these nonvertical flow components can be quantified when certain assumptions are made.

The LPMLE3 method uses a local polynomial (*LP*) model to separate periodic, nonperiodic (transient) and noise components contained in a temperature signal and to determine the system response in the frequency domain. The LP part [*Pintelon et al.*, 2010a] is combined with a maximum-likelihood estimator (*MLE*) to quantify the vertical flow component or thermal diffusivity and their uncertainties for finite streambed subdomains considering for each subdomain information from three (*3*) temperature sensors. Each subdomain has temperature boundary conditions (in form of temperature-time series) at its top and bottom, while the vertical flow component is estimated from a third sensor located within this domain. By using finite domains, vertical flow component and thermal parameters are considered locally constant over the entire subdomain.

The LP method is used here to determine transfer functions describing the system behavior. As such, it is similar to the one put forward in *Vandersteen et al.* [2015]. However, while *Vandersteen et al.* [2015] use the

transfer functions without transients, for LPMLE3 these transients are separated from the temperature measurements and their variances are utilized. Other researchers have used a local polynomial method to directly determine the Fourier transform of time series information [see *Li et al.*, 2011, for a review]. An *MLE3* without the LP part, which can only handle periodic input signals was introduced by *van Berkel et al.* [2014a]. Moreover, *van Berkel et al.* [2014a] and this work distinguish themselves also from *Vandersteen et al.* [2015] in that they consider noise on both the input and output temperature signals instead of only the output, making noise calculations more elaborate.

2. The LPMLE3 Method

2.1. The Analytical Solution

Coupled vertical (1-D) water flow and heat transport in a streambed can be defined after *Stallman* [1965] as:

$$\frac{\partial T}{\partial t} = D\frac{\partial^2 T}{\partial z^2} - q_z \frac{\rho_w c_w}{\rho c}\frac{\partial T}{\partial z} \tag{1}$$

with T [Θ] as the temperature depending on depth z [L] and time t [T]. The time-invariant parameters are the Darcy flux (streambed flux) q_z [$L\ T^{-1}$] along the z direction (here termed the vertical flow component), the volumetric heat capacity of water $\rho_w c_w$ [$ML^{-1}\ T^{-2}\ \Theta^{-1}$] and the volumetric heat capacity of the water-sediment matrix ρc [$ML^{-1}\ T^{-2}\ \Theta^{-1}$]. D [$L^2\ T$] in equation (1) is the effective thermal diffusivity that is calculated here as:

$$D = \frac{\kappa}{\rho c} \tag{2}$$

with κ [$ML\ T^{-3}\ \Theta^{-1}$] as the effective thermal conductivity of the saturated medium. While the second term of the right-hand side of equation (1) that includes the Darcy flux represents heat transport by convection (the movement of water), the first term represents heat transport by conduction in water and through the solid matrix. Several studies [see *Rau et al.*, 2014, for an extensive review] discuss the inclusion of an additional thermal dispersivity function in equation (2) that describes thermal dispersion due to the spatially variable water flow through the pores. However, this function will not be considered here as its impact on D seems often negligible in advection dominated systems [*Bons et al.*, 2013; *Rau et al.*, 2014], especially for fluxes smaller than around 10 m d^{-1} [*Rau et al.*, 2015].

The analytical solution to equation (1) for a semi-infinite halfspace is then given as:

$$T(z,t) = T_0(z,t) + Ae^{-az}\cos(\omega t - bz) \tag{3}$$

with A as the magnitude of the temperature amplitude at the upper boundary, ω as the angular frequency, and $T_0(z, t)$ [Θ] as the temperature without influence from a sinusoidal input signal. Parameters a and b are based on thermal characteristics of the streambed and the vertical flow component (see supporting information). Equation (3) has been applied in some form or other by many researchers [e.g., *Stallman*, 1965; *Goto et al.*, 2005; *Hatch et al.*, 2006; *Keery et al.*, 2007; *Luce et al.*, 2013] and assumes an upper boundary condition $T(z_1,t) = T_0(z,t) + A\cos(\omega t)$ while the location of the lower boundary condition $\lim_{z\to\infty} T(z_2,t) = T_0(z,t)$ is approaching infinity. As such, calculated vertical flow components or thermal parameters would be constant over the entire semi-infinite halfspace.

Solving equation (1) analytically to obtain vertical flow components or thermal parameters that vary with depth and are only constant between two temperature sensors is difficult. One possibility is to change the lower boundary condition to the second sensor, which means that equation (3) now becomes

$$T(z,t) = T_0(z,t) + Ae^{-az}\cos(\omega t - bz) + Ae^{az}\cos(\omega t + bz) \tag{4}$$

In this case two eigenfunctions need to be solved, and in order to obtain q_z and/or thermal parameters, information from a third temperature sensor is needed with $z_1 < z < z_2$, where z_1 and z_2 are the depths of the boundary sensors.

A second possibility is to solve equation (1) in the frequency domain by applying the Fourier transform $\mathscr{F}$ to obtain the (complex-valued) ordinary differential equation:

$$\frac{d^2\Theta}{dz^2}+\alpha\frac{d\Theta}{dz}+(i\omega\gamma)\Theta=0 \tag{5}$$

with $\Theta = \mathscr{F}\{T\}$, and $i=\sqrt{-1}$, while α and γ contain information on q_z and thermal parameters as shown in the supporting information. In case of periodic signals and without considering additional noise the analytical solution to equation (5) would then become

$$\Theta(z,\omega,\theta)=C_1e^{(\lambda_1 z)}+C_2e^{(\lambda_2 z)} \tag{6}$$

with the parameter vector $\theta = [\alpha\ \gamma]$, where

$$\lambda_{1,2}=\frac{1}{2}\left(-\alpha\pm\sqrt{\alpha^2-4i\omega\gamma}\right) \tag{7}$$

C_1 and C_2 in equation (6) are determined using measured temperatures $\Theta(z = z_1)$ and $\Theta(z = z_2)$ from the boundary sensors (see supporting information for further explanation).

2.2. The LP Part

To obtain θ one can relate the predicted output $\Theta(z, \omega, \theta)$ from equation (6) to actual temperature measurements $\Theta_{meas}(z, \omega)$ by, e.g., using a MLE. However, as measured temperature signals often contain periodic and nonperiodic parts (due to slow temperature fluctuations or instrument drift) and are perturbed with noise, methods are needed that separate these parts from the measured input spectra before parameter estimation can be performed (see supporting information).

One of these methods is the LP method [*Pintelon et al*., 2010a, 2010b; *Vandersteen et al*., 2015], which uses the concept of transfer functions or frequency response functions (FRFs). These FRFs describe the system for every frequency and depth. The LP method assumes that between sensors thermal transport is linear, which follows directly from equation (1). Also, a noiseless reference temperature is assumed to exist, e.g., obtained from a temperature sensor at the streambed top. Between this reference temperature and any temperature at a certain depth z a (nonparametric) transfer function can then be estimated.

Transients and other low-frequent disturbances result in smooth decaying functions in the (complex-plane) frequency domain, unlike the temperature fluctuations such as the diel cycle and noise. As the smoothness and order of these functions is unknown, they are locally approximated using only a number of discrete spectral lines and a low order (local) polynomial. The order of the polynomial is determined by analyzing the residuals (least square errors) resulting from fitting the polynomial function to the spectral lines used. If the residuals become larger, the quality of the approximation decreases. In most cases, such as the examples discussed later on, a second order polynomial is sufficient.

2.3. The MLE3 Part

In the next step, the LPMLE3 method uses the obtained FRFs and the noise information on these FRFs as input to a MLE to estimate the parameter vector $\hat{\theta}=[\hat{\alpha}\ \hat{\gamma}]$ (indicated by the accent above the symbols). The general idea behind the MLE is to maximize a known likelihood function, in our case the probability density function with respect to the measurements. $\hat{\theta}$ is then determined by minimizing a log-likelihood cost function $V_{ML}(\theta, \omega_k)$ by means of nonlinear least squares optimization techniques as outlined in *van Berkel et al*. [2014a] via

$$\hat{\theta}=\min_{\theta}V_{ML}(\theta,\omega_k) \tag{8}$$

where ω_k are those frequencies determined by the LP method with a significant signal-to-noise ratio (see supporting information) and

$$V_{ML}(\theta,\omega_k)=\frac{1}{F}\sum_{k=1}^{F}|e_{ML}(\theta,\omega_k)|^2 \tag{9}$$

where F is the number of spectral lines used in the estimation. The estimation error $e_{ML}(\theta,\omega_k)$ is calculated as:

$$e_{ML}(\theta, \omega_k) = \frac{\Theta(z, \omega_k, \theta) - \Theta_{meas}(z, \omega_k)}{\sigma_e(\theta, \omega_k)} \tag{10}$$

where $\sigma_e(\theta, \omega_k)$ is the variability (in this case the standard deviation) that considers the different noises (see supporting information).

To minimize the cost function, we used an analytical Jacobian matrix as put forward in *van Berkel et al.* [2014a]. This Jacobian matrix can also be used to determine the covariance matrix $COV(\hat{\theta})$ of $\hat{\theta} = [\hat{\alpha}\ \hat{\gamma}]$. The MLE concept can then be applied to quantify $\hat{q}_z$ and $\hat{D}$ according to

$$\hat{q}_z = \frac{\hat{\alpha}}{\hat{\gamma}} \frac{\rho c}{\rho_w c_w} \tag{11}$$

$$\hat{D} = -\frac{1}{\hat{\gamma}} \tag{12}$$

The uncertainties on $\hat{q}_z$ and $\hat{D}$ can be calculated with the covariance matrix $COV(\hat{q}_z, \hat{D})$ via

$$COV(\hat{q}_z, \hat{D}) = J^h_{\theta \to \theta'} COV(\hat{\theta}) J_{\theta \to \theta'} \tag{13}$$

where $J_{\theta \to \theta'}$ is the Jacobian matrix

$$J_{\theta \to \theta'} = \begin{bmatrix} \frac{1}{\hat{\gamma}} \frac{\rho c}{\rho_w c_w} & -\frac{\hat{\alpha}}{\hat{\gamma}^2} \frac{\rho c}{\rho_w c_w} \\ 0 & \frac{1}{\hat{\gamma}^2} \end{bmatrix} \tag{14}$$

and $J^h_{\theta \to \theta'}$ its Hermitian transpose. The estimated parameters $\hat{q}_z$ and $\hat{D}$ are only valid results for the respective streambed subdomain, for which temperature data has been used. Aspects regarding the optimal distance between sensors are discussed by *van Berkel et al.* [2014a]. They point out that parameter estimates improve with increasing distance between upper and lower boundary, as the attenuation of the temperature signal is more pronounced (the signals still need to be significantly large to have a significant signal-to-noise ratio). On the other hand, as the subdomain size increases, the assumption of constant flux and thermal parameters may become increasingly problematic.

A helpful tool to detect model structure errors (i.e., to see whether the assumption of 1-D vertical water flow and heat transport is adequate) is a cost function analysis. Such analysis describes the goodness of fit between the actual model used and a theoretical one. In our case, a theoretical expected value V_E of the cost function based on the degrees of freedom can be compared to the actual value V_{ML} obtained from equation (9). The expected cost function value, i.e., the degrees of freedom can be obtained as [*van Berkel et al.*, 2014a]

$$V_E = \left(F - \frac{n}{2}\right) \tag{15}$$

where n is the number of (unknown) free parameters (e.g., $\hat{q}_z$ and $\hat{D}$) and F again the number of spectral lines, which fixes two degrees of freedom (real and complex or amplitude and phase). *van Berkel et al.* [2014a] suggest that a model is acceptable if V_{ML} falls within a 95% confidence interval around V_E. When V_{ML} falls outside this range it might be useful to decrease the distance between upper and lower boundary. However, smaller subdomains increase the uncertainty on the parameter estimates and hence a compromise needs to be made.

3. Method Application and Verification

We implemented the LPMLE3 method in MATLAB 2011b® (The MathWorks, Inc., Natick, MA, USA) and tested its applicability using two data sets. First, we show by using a synthetic data set created with the numerical model STRIVE that the LPMLE3 method is able to extract known vertical flow components and thermal diffusivities with little error. Afterwards, we calculate vertical flow components for a temperature-time series obtained from the Slootbeek, a small stream in Belgium and show how this information could be used to delineate nonvertical flow components.

3.1. Verification Using Simulated Data

The LP and MLE3 parts were extensively tested by *Pintelon et al*. [2010a, 2010b] and *van Berkel et al*. [2014a], respectively; Monte-Carlo analyses conducted by them showed that the uncertainties can be well predicted. To investigate the performance of LPMLE3, we used a temperature distribution (i.e., a set of many time series) with depth created with the 1-D finite difference model STRIVE [*Anibas et al*., 2009; *Vandersteen et al*., 2015]. This model uses the numerical approach put forward by *Lapham* [1989] and can deduce vertical flow by inverse modeling of temperature data. For this, it can be operated in steady state or transient mode as described by *Anibas et al*. [2009].Water storage in the streambed is neglected. By assuming upwelling flow conditions ($q_z = -86.40$ mm d^{-1}) and a thermal diffusivity of $D = 8.333 \times 10^{-7}$ m^2 s^{-1} as described in the supplement, we used STRIVE to calculate a distribution of the temperature in the HZ with time assuming strictly vertical flow. The upper boundary used was a measured temperature-time series obtained from the Aa River, Belgium [*Anibas et al*., 2009], covering 520 days. The lower boundary was defined by the average regional groundwater temperature of 12.2°C at 5 m depth. The temperature distribution between upper and lower boundary was calculated with STRIVE for every 0.01 m. For seven successive streambed subdomains (0.1–0.2, 0.2–0.3, . . ., 0.7–0.8 m; with the third sensor always in the middle), STRIVE temperatures were used as input to the LPMLE3 model to quantify vertical flow and thermal diffusivities. For that, two cases were defined: (i) the LPMLE3 method was used with only a frequency of 1 d^{-1} as is common in studies using amplitude/phase lag methods, and (ii) the LPMLE3 method was used with a frequency range from 1/520 to 1.5 d^{-1}. Frequencies larger than 1.5 d^{-1} did not have a significant influence on estimates of the vertical flow component. In general, the frequency range used in the LPMLE3 method can be chosen freely by the user, whose choice will depend on the length and information content of the data set, as well as the purpose of the investigation. The frequency range used can affect the outcome of the parameter estimation as has been shown by *Vandersteen et al*. [2015] in section 3.5 and Figure 7.

For case (i), q_z obtained with the LPMLE3 method deviated between 0.15% and 1.32% from the STRIVE value of -86.40 mm d^{-1} (Figure 2, supporting information Table S1), while estimated diffusivities differed between 0.25% and 1.98% (supporting information Table S1). Although deviations are small, they increase with depth and both parameters are slightly overestimated. This is a result from the attenuation of the daily temperature signal with depth. Although this daily signal is by far the most pronounced one in the upper streambed, lower frequencies increase their influence on q_z estimates with increasing depth. For case (ii), an increased parameter variation with depth could not be observed. Vertical flow components deviated between 0.00% and 0.10% while estimated D deviated between 0.00% and 0.05% (supporting information Table S2). Standard deviations on the parameter estimates increased with depth but for case (ii) they were 2–3 orders of magnitude smaller compared to case (i). The small differences of q_z and D for case (ii) as compared to the values obtained from the simulations with STRIVE can be a result from truncation of the temperature data (after the third digit) during extraction from the STRIVE model. Additionally, numerical errors produced by STRIVE when approximating the partial differential equation for heat transport on a grid could have had an influence.

When performing a cost function analysis for case (ii), the expected value of the cost function was found to be 779 (i.e., 520 days multiplied with the highest frequency used, which is 1.5 d^{-1} in this case. The result is subtracted by 1, i.e., the number of free parameters divided by two, see equation (15)). The actual model cost (CostBest) values were between 22% and 438% higher than the expected cost value. For a field data set one could assume that these differences are due to the influence of horizontal flow components that would make the assumption of 1-D vertical flow increasingly less valid. However, for the synthetic data set the temperature-time series output created with STRIVE is noiseless and the actual model cost is dominated by numerical errors and not the noise contained in the temperature signal. By increasing the noise, actual and expected cost values would differ less.

As a comparison, Figure 2 also shows estimates of q_z obtained with the semi-infinite amplitude method of *Hatch et al*. [2006] as implemented in VFLUX version 1.2.3 [*Gordon et al*., 2012]. From the deviations it can be seen that using the amplitude method to calculate depth-dependent q_z can lead to noticeable errors. In our case q_z estimates from VFLUX deviated between 1.15% and 11.27% (supporting information Table S3) from -86.40 mm d^{-1}. Considering these results, we conclude that the LPMLE3 method is usable for the quantification of vertical flow components and thermal diffusivities. Moreover, the results also show that methods like LPMLE3 have advantages over amplitude/phase lag methods.

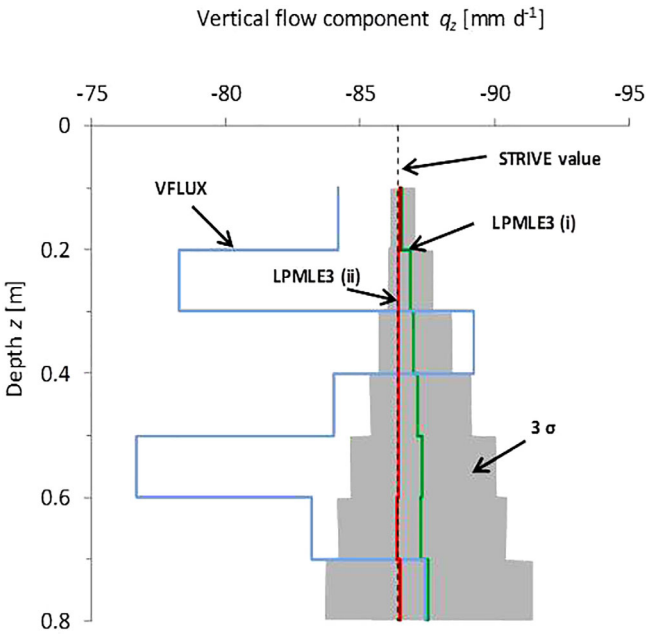

Figure 2. Estimates of the vertical flow component versus depth obtained with the LPMLE3 method and VFLUX version 1.2.3. The latter was used with the amplitude method after *Hatch et al.* [2006]. LPMLE3 (i) results were calculated using only a frequency of 1 d^{-1}. LPMLE3 (ii) results were obtained using a frequency range as defined in the text. The uncertainty bounds 3σ are shown for LPMLE3 (i) only. For LPMLE3 (ii) they were too small to be visible on the figure. LPMLE3 (ii) reproduces the original STRIVE value of −86.4 mm d^{-1} (dotted black line) most accurately. VFLUX results were obtained using a frequency of 1 d^{-1}. As VFLUX produces one estimate per day, vertical flow components were averaged for each depth.

3.2. Vertical and Nonvertical Flow Components at the Slootbeek Field Site

3.2.1. Field Site and Measurements

Temperature-time series were recorded at location ML6 in the Slootbeek (51°12′36.6″N 4°50′14.9″E), a small lowland stream of around 4 km length in North-Eastern Belgium (Figure 3) and tributary to the Aa River. The Slootbeek is fed by several drainage canals and its stream stage is heavily influenced by its location in an agricultural landscape [*Anibas et al.*, 2016]. The streambed is composed predominantly of fine sand and silt with varying content of organic matter at the top and occasional gravel deposits. The organic matter content increases downstream. Average discharge at the confluence with the Aa River is about 0.05 m^3 s^{-1} [*De Doncker*, 2010] and average stream velocity during installation of the measurement equipment was about 0.2 m s^{-1}. ML6 was located about 120 m upstream of the confluence with the Aa River and equipped with a temperature probe [*Schmidt et al.*, 2014] containing a data logger from UIT, Dresden, Germany (Figure 4). The temperature probe is composed of a solid rod of polyoxymethylene. It has a total length of 0.66 m (Figure 4), an outer diameter of 0.02 m and holds eight TSIC-506 temperature sensors with variable sensor spacing. The sensors are semiconducting resistors embedded in an integrated circuit. The accuracy of the temperature sensors is 0.07°C for a temperature range of 5–45°C and their resolution is 0.04°C. Thin stainless steel flat blanks of 9 mm diameter are inserted into the plastic rod at the sensor locations to ensure optimal thermal contact with the surrounding material. The temperature probe was calibrated in a water bath to allow for corrections of sensor inaccuracies. The temperature probe simultaneously measured temperatures at the

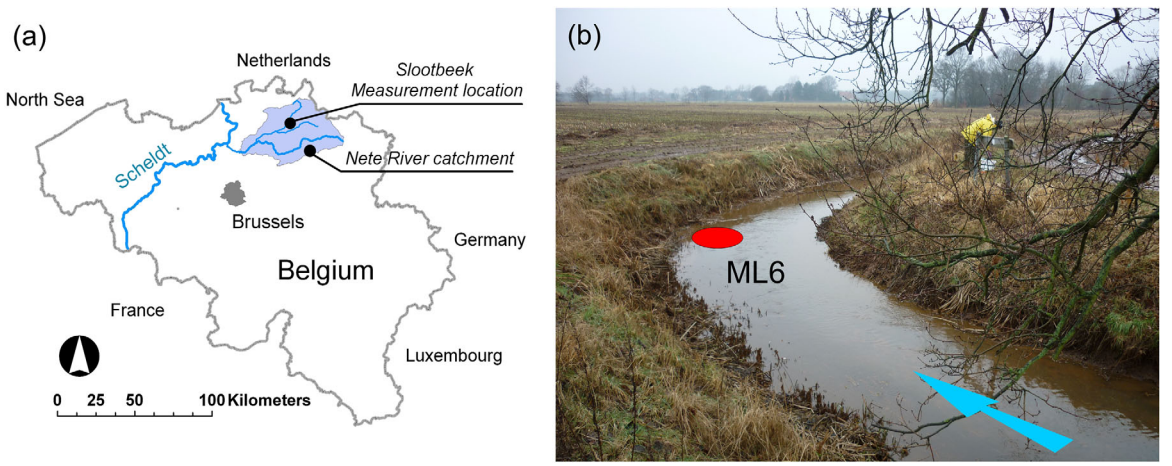

Figure 3. (a) The Slootbeek is a small tributary to the Aa River and part of the Nete River catchment in Northern Belgium. (b) Streambed temperatures were measured at location ML6 in the Slootbeek at the outside of a stream bend.

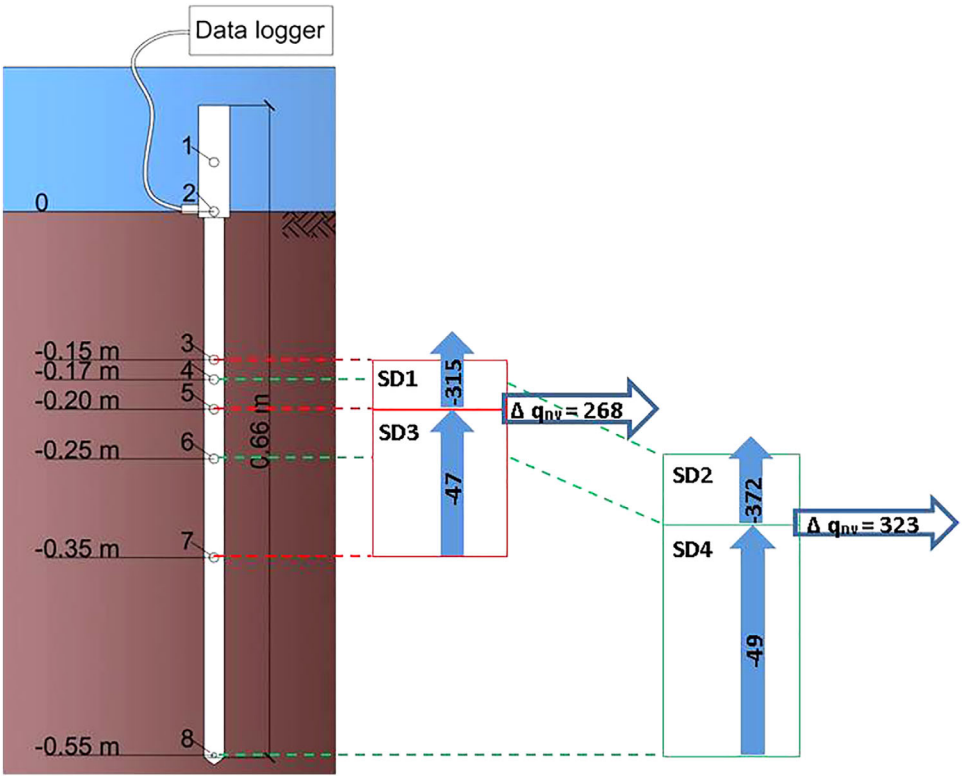

Figure 4. Estimates of the vertical flow component for ML6 based on temperature data collected with a temperature probe from UIT, Dresden, Germany [*Schmidt et al.*, 2014] between 17 February and 17 May 2012. Data from sensor 1 were not used for our analyses. Sensor two was located at the streambed top and the other sensors were placed within the streambed at known distances. Vertical flow components (indicated by solid blue upward arrows) were estimated with the LPMLE3 method for all streambed subdomains, including nonoverlapping subdomains SD1 and SD3 as well as SD2 and SD4 that are shown here. Estimates vary with depth and subdomain size. Differences in vertical flow between subsequent subdomains (indicated by the blue arrows pointing to the right) indicate a change in the magnitude of the nonvertical flow component. The direction of the nonvertical flow component cannot be delineated. All values are in mm d^{-1} (see also Table 1).

streambed top and at depths of 0.15, 0.17, 0.20, 0.25, 0.35, and 0.55 m over a period of 90 days (17 February to 17 May 2012) with an interval of 10 min. Further details about the field site, the measurement setup and additional measurements can be found in *Anibas et al.* [2016].

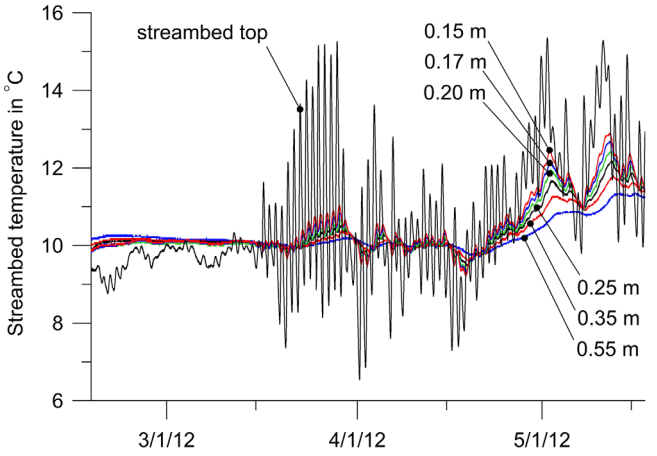

Figure 5. Temperature data collected at location ML6 at the streambed top and six depths.

3.2.2. Estimating Vertical Flow Components

The temperature data (Figure 5) from location ML6 (Figure 3) were used to estimate the vertical flow components with the LPMLE3 method. Over the 90 day observation period, temperatures ranged from 6.5 to 15.4°C with an average of 10.4°C and a standard deviation of 0.8°C. The sensor at the streambed top showed the highest temperature fluctuations due to the influence of the diel cycle while the temperature signal was attenuated with increasing distance from the streambed top. From February until Mid-March, temperature fluctuations

Table 1. Estimates of Vertical Flow Components q_z and Their Uncertainties for Different Streambed Subdomains Using Sensor-Triplets With Consecutive and Nonconsecutive Numbering From the Temperature Probe Shown in Figure 4 at Location ML6[a]

Subdomain	Sensors	Size (m)	q_z (mm d^{-1})	σ_{qz} (mm d^{-1})	σ_{qz} (%)	CostBest	q_{nv} (mm d^{-1})	Range q_{nv} (mm d^{-1})
SD1	3-4-5	0.05	−315	18.6	5.9	259	213	207–219
SD2	4-5-6	0.08	−372	12.0	3.2	265	156	142–170
SD3	5-6-7	0.15	−47	7.8	16.6	215	481	454–507
SD4	6-7-8	0.3	−49	4.2	8.5	126	479	442–516
SD5	3-4-6		−304	8.1	2.7	331	224	198–249
	3-5-6		−340	6.8	2	317	188	158–217
SD6	3-4-7	0.2	−229	6.4	2.8	431	299	268–329
	3-5-7		−218	3.5	1.6	588	310	270–349
	3-6-7		−147	4.0	2.7	453	381	343–419
SD7	3-4-8	0.4	−168	5.4	3.2	517	360	326–393
	3-5-8		−159	3.4	2.1	701	369	329–408
	3-6-8		−105	3.2	3.1	422	423	383–463
	3-7-8		−81	2.7	3.3	165	447	405–489
SD8	4-5-7	0.18	−210	6.3	3	366	318	287–349
	4-6-7		−126	4.2	3.4	343	402	365–439
SD9	4-5-8	0.38	−158	5.1	3.2	367	370	335–404
	4-6-8		−90	3.4	3.8	273	438	398–477
	4-7-8		−68	3.0	4.4	117	460	419–501
SD10	5-6-8	0.35	−45	5.0	11.1	204	483	448–518
	5-7-8		−49	3.1	6.3	94	479	438–519

[a]Based on these q_z estimates and making certain assumptions (see section 3.2.3), nonvertical flow components q_{nv} were delineated for each subsection. Size = size of streambed subdomain; q_z = estimated vertical flow component; σ_{qz} = standard deviation of q_z; CostBest = actual value of cost function analysis, the expected value is 134; q_{nv} = nonvertical flow component; Range q_{nv} = range of the nonvertical flow component if $\pm 3 \times \sigma_{qz}$ is added to q_z.

were much less pronounced than afterwards. For calculations of the vertical flow components the thermal diffusivity was fixed to 4.375 × 10^{-7} m^2 s^{-1}, a value accounting for the organic matter content at ML6 [*Anibas et al.*, 2016]. This was done as independent field measurements of thermal parameters were not available.

For the temperature probe shown in Figure 4 and assuming sensor 2 (at the streambed top) as the noiseless reference sensor, vertical flow components can be estimated for 10 streambed subdomains (SD1 to SD10, Table 1) using sensor triplets either with consecutive (e.g., 3-4-5) or nonconsecutive numbering (e.g., 3-4-6). For each triplet the first and third sensors represent the upper, respectively lower boundary of the subdomain while the second sensor shows the system response. For these 10 subdomains, the vertical flow component varied between −45 mm d^{-1} for SD10 (sensors 5-6-8) and −372 mm d^{-1} for SD2, always indicating upwelling conditions. For subdomains with estimates based on more than one possible sensor combination (e.g., SD7), estimates significantly decreased in most cases (except for SD5 and SD10) with increasing depth of the sensor showing the system response. In those cases, it might be appropriate to use average vertical flow estimates for further analysis.

Percent standard deviations ranged from 1.6% for SD6 (sensors 3-5-7) to 16.6% for SD3. They were higher for subdomains starting at or below sensor five. This is probably a result of the attenuation of the temperature signal with depth, which makes estimates of the vertical flow component in general more uncertain using these heat tracing methods. In comparison, estimates obtained with the LPML method as described by *Vandersteen et al.* [2015], who assume the entire subsurface to be a homogeneous semi-infinite halfspace amount to −312 mm d^{-1} with an uncertainty on the estimate of 1.2 mm d^{-1} or 0.4%. This value would be most comparable to estimates for SD1, SD2, and SD5.

Figure 4 shows the temperature probe and estimates of the vertical flow components for subsequent subdomains SD1 and SD3 as well as SD2 and SD4. Whereas SD1 and SD2 show estimates for q_z of −315 and −372 mm d^{-1}, respectively, estimates for SD3 and SD4 are much smaller with −47 and −49 mm d^{-1}, respectively. Such a decrease in the vertical flow component with increasing distance from the streambed top has already been described in previous studies [e.g., *Roshan et al.*, 2012; *Irvine et al.*, 2015b]. The estimates of vertical flow can be used in further analyses (not contained in the LPMLE3 code) to delineate nonvertical flow components.

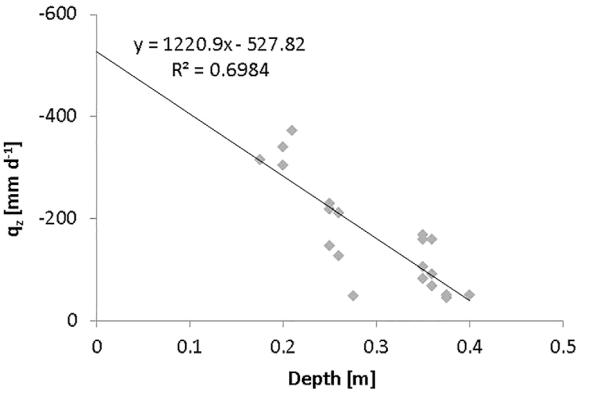

Figure 6. To determine nonvertical flow components for subdomains of ML6, we assumed that (i) the decrease of the vertical flow component with depth close to the streambed top could be approximated linearly and (ii) that at depth $z = 0$ only vertical flow occurs. All q_z estimates listed in Table 1 were used in linear regression. They were assigned to the center depth of each subdomain. With a Pearson correlation coefficient of $r = 0.84$ the assumption of a linear behavior seems adequate.

3.2.3. Nonvertical Flow Components

Vertical flow components presented in Table 1 show considerable variation for the different streambed subdomains. However, their expected magnitudes should be equal for all subdomains if flow in the system was considered purely vertical and if conservation of mass is to be ensured. We thus hypothesize that these variations between subdomains are mainly due to the existence of nonvertical flow components. Such nonvertical flow components have been found to increase with increasing distance from the streambed top [*Roshan et al*., 2012; *Cranswick et al*., 2014] as well as increasing streambed heterogeneity [*Irvine et al*., 2015b]. *Lautz* [2010], *Roshan et al*. [2012], and *Cranswick et al*. [2014] showed in modeling studies that nonvertical flow components can produce substantial errors in vertical flux estimates obtained with 1-D methods if the vertical flow component is near zero. *Irvine et al*. [2015b] demonstrated that variations in vertical flux estimates were large, when horizontal flow components were dominant as compared to vertical components. *Cuthbert and Mackay* [2013] on the other hand showed that the existence of a nonvertical flow component alone does not necessarily produce erroneous vertical flux estimates. Instead, they found increasing errors in estimates of the vertical flow component for strongly nonuniform flow fields, where many converging/diverging flow lines exist due to the influence of shallow hyporheic exchange flow.

By assuming conservation of mass, SD3 has a nonvertical flow component that is higher by 268 mm d^{-1} than that of SD1 (based on the q_z estimates discussed in section 3.2.2). Accordingly, SD4 has a nonvertical flow component that is larger by 323 mm d^{-1} than that of SD2. However, determining the magnitude of the nonvertical flow component of each subdomain does not seem straight-forward as the distribution of the vertical flow component with depth is generally not known. In case of ML6, all vertical flow components are directed upwards (Table 1). We thus assumed that at depth $z = 0$ only vertical flow occurs and used linear regression on the q_z estimates listed in Table 1 as shown in Figure 6. Values were assigned to the center depth of each subdomain. With a Pearson correlation coefficient of $r = 0.84$ the assumption of a linear behavior seems adequate. However, a linear decrease of the vertical flow component with depth should by no means be understood as generally valid and should be checked carefully. At distances farther away from the streambed top or when the vertical flow vector frequently changes direction, linear regression will most probably not prove useful.

For ML6, at $z = 0$, the vertical flow estimate would then be $^{-}$528 mm d^{-1} and nonvertical flow would be 0. To allow for mass conservation, the overall flow must be constant and is then the sum of the vertical and nonvertical flow components. As such we could deduce the magnitudes of the nonvertical flow component q_{nv} over each subdomain (Table 1). They vary between 156 mm d^{-1} (SD2) and 483 mm d^{-1} (SD10, sensors 5-6-8). By including the uncertainty on the q_z estimates as $\pm 3 \times \sigma_{qz}$ (see Table 1), linear regression on the lowest and highest q_z estimates could be performed (supporting information Figures S1 and S2) and for each subdomain, ranges of q_{nv} could be deduced (Table 1). The smallest range was encountered for subdomain SD1, while the largest range was encountered for SD7 (sensors 3-7-8). The CostBest values shown in Table 1 as a measure for model performance differ between 70% and 523% from the expected value of 134 and no trend is visible if compared to the magnitudes of the nonvertical flow component.

3.2.4. Other Factors Influencing Vertical Flow Estimates

Aside from the existence of nonvertical flow components or a nonuniform flow field, errors in vertical flow estimates could arise from the quality of the temperature data. On the one hand, this quality is influenced by sensor accuracy [*Shanafield et al*., 2011] and resolution [*Soto-Lopez et al*., 2011]. In our study, we reduced

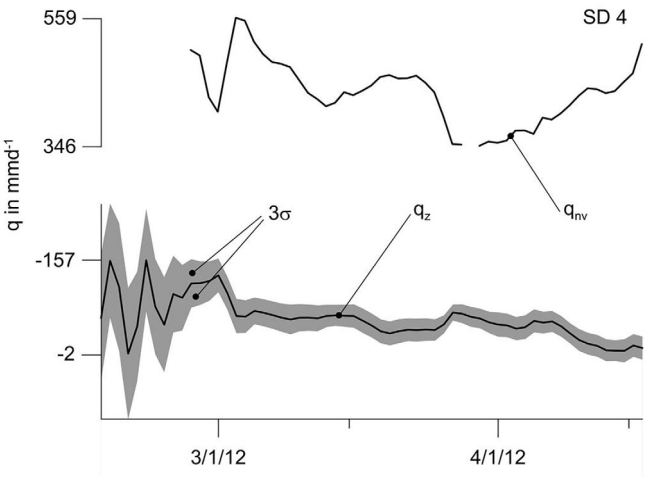

Figure 7. Temporal variability of the vertical flow component q_z (black dotted line) and its uncertainty (3σ; gray bands) for streambed subdomain SD4 after applying a 30 day window on the temperature-time series. The magnitude of the nonvertical flow component q_{nv} was obtained by performing linear regression (see Figure 6) on q_z estimates for each period. Only those nonvertical flow components are shown, where the Pearson correlation coefficient $r > 0.6$.

the impact of measurement errors by calibrating the multilevel temperature stick in a water bath of known temperature. Also, initial accuracy was equal for all sensors. On the other hand, the temperature signal is generally attenuated with increasing depth and at deeper sensors often less information can be used for parameter estimation. The modeling process itself could also add errors to the q_z estimates. For example, for a reasonably small subdomain, the boundary temperature sensors, as well as measurement and parameterization errors could potentially have an influence on the estimates. Further research is needed to quantify these potential error sources.

3.2.5. Estimating Time-Variant Flow Components

To study the temporal variability of vertical flow components, the LPMLE3 method was used on parts of the temperature-time series from location ML6 by applying a moving window and the Short Time Fourier Transform. In general, the window length can be selected freely depending on the used frequency information; however the same limitations apply as to the LPML method [*Pintelon et al*., 2010a; *Vandersteen et al*., 2015]. The shorter the window, the better the temporal resolution but also the noisier the output signal will be. At least two complete periods of data (in our case 2 days) are needed to estimate the FRFs and the transient parts. When a frequency range is used, the longer the window the smoother the vertical flow curves will appear as more small frequencies (i.e., longer periods) can be included in the analysis. For illustration purposes, we applied a 30 day rectangular moving window on subdomain SD4 (Figure 7) using frequencies of up to 1.5 d^{-1} and assumed a constant thermal diffusivity of 4.375×10^{-7} m^2 s^{-1}. The window was always moved by one day.

For SD4 (0.25–0.55 m depth), vertical flow components varied between -2 and -157 mm d^{-1}, with stronger fluctuations occurring during the first part of the time series. Percent standard deviations (σ) ranged from 6% to 2430%, with the highest uncertainties occurring near zero vertical flow. They are also larger at the beginning of the q_z-time series than after Mid-March. This coincides with a different temperature pattern (Figure 5) showing less variation, which seemingly makes parameter estimation for the model more challenging. Figure 7 also shows a time series of the nonvertical flow components assuming again that the decrease of the vertical flow component with depth can be approximated linearly and regression analysis can be performed. In fact, the Pearson correlation coefficient varied between 0.04 and 0.89, indicating that not for all cases correlation can be assumed linear. The graph in Figure 7 shows thus only those q_{nv} estimates where the Pearson correlation coefficient was above 0.6 (84% of the cases). These nonvertical flow components ranged from 346 to 559 mm d^{-1}.

4. Conclusions

The LPMLE3 method is a new approach to quantify vertical flow components in streambeds using temperature-time series collected in streambed sediments. The LPMLE3 method solves the vertical 1-D partial differential heat transport equation after *Stallman* [1965] in the frequency domain. Unlike other methods [e.g., *Hatch et al*., 2006; *Keery et al*., 2007; *Luce et al*., 2013; *Vandersteen et al*., 2015] that are based on the assumption of a semi-infinite domain with the location of the lower boundary approaching infinity, the LPMLE3 method uses a local lower boundary condition. As such, the streambed can be divided into finite subdomains, that are bound above and below by temperature-time series, while temperature information from a third sensor within the subdomain is used for parameter estimation. The advantage of this approach

is that resulting vertical flow estimates and thermal parameters are only considered constant in the subdomain and not over the entire semi-infinite halfspace. The LPMLE3 method combines a local polynomial systems model and a MLE. The local polynomial model separates a temperature signal into periodic, nonperiodic (transient), and noise parts and their variances. The MLE is used for parameter estimation and via a covariance analysis uncertainties on the parameter estimates can be determined quickly. The presented results show that the LPMLE3 method can serve as a tool to estimate vertical flow components in streambed subdomains when temperatures are measured at many depths simultaneously with a multilevel temperature measurement device.

LPMLE3 provides information regarding the vertical water flow component within a certain finite subdomain. Differences in this vertical flow component between nonoverlapping subdomains might indicate a larger or smaller contribution of nonvertical flow and identify zones where nonvertical flow dominates vertical flow (e.g., SD4). A direct quantification of the nonvertical flow component of each subdomain, however, is not trivial as the decrease of the vertical flow component with depth is not known. By conducting additional analyses and by making certain assumptions (linear decrease of the vertical flow component with distance from the streambed top, mass conservation) we could quantify the nonvertical flow components for our field data. These assumptions will likely not hold true for all stream environments, e.g., where the temperature probe cuts through more than one flow path as discussed by *Briggs et al*. [2012]. If one would be interested in more robust estimates of these nonvertical flow components it might be worthwhile considering the use of 2-D or 3-D models or active heat sensors such as the one shown by *Lewandowski et al*. [2011] and *Angermann et al*. [2012] or heated FO-DTS systems [*Striegl and Loheide*, 2012].

With this in mind, future studies could further elaborate on the importance of nonvertical flow components in the hyporheic zone and their effect on flow and transport processes as well as groundwater-surface water interaction. The general suitability of 1-D heat methods to quantify representative exchange fluxes might also need further clarification. From a methodological point of view, the LPMLE3 method could be applied on temperature data with variable spatial density to study limitations regarding subdomain size. For practitioners interested in the temporal variability of vertical flow components, future studies could also investigate the interplay between the size of the subdomain, temperature data quality and the windowing technique applied. The use of the LPMLE3 method with temperature data from different environments could further strengthen its potential applicability.

Acknowledgments
The LPMLE3 code can be obtained from the corresponding author upon request. The code will be made publicly available for download in the near future. Data used to produce Figure 2 can be found in the supporting information (supporting information Tables S1–S3). All other data can be obtained upon request. U. Schneidewind completed a major part of his contribution within the framework of the Marie Curie Initial Training Network ADVOCATE—Advancing sustainable *in situ* remediation for contaminated land and groundwater, funded by the European Community's Seventh Framework Programme (*FP7/2007-2013* under grant 265063). M. van Berkel carried out his part with financial support from NWO within the framework of the EUROfusion Consortium. He also received funding from the Euratom research and training program 2014–2018 under grant 633053. For G. Vandersteen, this work was sponsored by the Strategic Research Program of the VUB (SRP-19), the Institute for the Promotion of Innovation through Science and Technology in Flanders (IWT-Vlaanderen), Fund for Scientific Research (FWO-Vlaanderen), the Flemish Government (Methusalem), and the Belgian Federal Government (IUAP VI/4). The views and opinions expressed herein do not necessarily reflect those of the funding agencies. This study was supported by TERENO (Terrestrial Environmental Observatories). We would like to thank three anonymous reviewers and the associate editor Erich T. Hester for their invaluable comments and ideas on how to improve the manuscript and deal with the aspect of nonvertical flow.

References

Alexander, M. D., and D. Caissie (2003), Variability and comparison of hyporheic water temperatures and seepage fluxes in a small Atlantic salmon stream, *Ground Water*, *41*(1), 72–82.

Anderson, M. P. (2005), Heat as a ground water tracer, *Ground Water*, *43*(6), 951–968, doi:10.1111/j.1745-6584.2005.00052.x.

Angermann, L., S. Krause, and J. Lewandowski (2012), Application of heat pulse injections for investigating shallow hyporheic flow in a lowland river, *Water Resour. Res.*, *48*, W00P02, doi:10.1029/2012WR012564.

Anibas, C., J. H. Fleckenstein, N. Volze, K. Buis, R. Verhoeven, P. Meire, and O. Batelaan (2009), Transient or steady-state? Using vertical temperature profiles to quantify groundwater-surface water exchange, *Hydrol. Processes*, *23*(15), 2165–2177, doi:10.1002/hyp.7289.

Anibas, C., U. Schneidewind, G. Vandersteen, I. Joris, P. Seuntjens, and O. Batelaan (2016), From streambed temperature measurements to spatial-temporal flux quantification: Using the LPML method to study groundwater-surface water interaction, *Hydrol. Processes*, *30*, 203–216, doi:10.1002/hyp.10588.

Bardini, L., F. Boano, M. B. Cardenas, A. H. Sawyer, R. Revelli, and L. Ridolfi (2013), Small-scale permeability heterogeneity has negligible effects on nutrient cycling in streambeds, *Geophysical Res. Lett.*, *40*, 1118–1122, doi:10.1002/grl.50224.

Barlow, J. R. B., and R. H. Coupe (2009), Use of heat to estimate streambed fluxes during extreme hydrologic events, *Water Resour. Res.*, *45*, W01403, doi:10.1029/2007WR006121.

Bartsch, S., S. Frei, M. Ruidisch, C. L. Shope, S. Peiffer, B. Kim, and J. H. Fleckenstein (2014), River-aquifer exchange fluxes under monsoonal climate conditions, *J. Hydrol.*, *509*, 601–614, doi:10.1016/j.jhydrol.2013.12.005.

Bianchin, M., L. Smith, and R. Beckie (2010), Quantifying hyporheic exchange in a tidal river using temperature time series, *Water Resour. Res.*, *46*, W07507, doi:10.1029/2009WR008365.

Boano, F., J. W. Harvey, A. Marion, A. I. Packman, R. Revelli, L. Ridolfi, and A. Wörman (2014), Hyporheic flow and transport processes: Mechanisms, models, and biogeochemical implications, *Rev. Geophys.*, *52*, 603–679, doi:10.1002/2012RG000417.

Bons, P. D., B. P. van Milligen, and P. Blum (2013), A general unified expression for solute and heat dispersion in homogeneous porous media, *Water Resour. Res.*, *49*, 6166–6178, doi:10.1002/wrcr.20488.

Briggs, M. A., L. K. Lautz, J. M. McKenzie, R. P. Gordon, and D. K. Hare (2012), Using high-resolution distributed temperature sensing to quantify spatial and temporal variability in vertical hyporheic flux, *Water Resour. Res.*, *48*, W02527, doi:10.1029/2011WR011227.

Briggs, M. A., L. K. Lautz, D. K. Hare, and R. González-Pinzón (2013), Relating hyporheic fluxes, residence times, and redox-sensitive biogeochemical processes upstream of beaver dams, *Freshwater Sci.*, *32*(2), 622–641, doi:10.1899/12-110.1.

Bukaveckas, P. A. (2007), Effects of channel restoration on water velocity, transient storage, and nutrient uptake in a channelized stream, *Environ. Sci. Technol.*, *41*(5), 1570–1576, doi:10.1021/es061618x.

Buss, S. R., et al. (2009), The Hyporheic Handbook—A handbook on the groundwater-surface water interface and hyporheic zone for environmental managers, *Sci. Rep. SC50070*, 280 pp., Environment Agency, Bristol.
Conant, B., Jr. (2004), Delineating and quantifying ground water discharge zones using streambed temperatures, *Ground Water*, *42*(2), 243–257, doi:10.1111/j.1745-6584.2004.tb02671.x.
Cranswick, R. H., P. G. Cook, M. Shanafield, and S. Lamontagne (2014), The vertical variability of hyporheic fluxes inferred from riverbed temperature data, *Water Resour. Res.*, *50*, 3994–4010, doi:10.1002/2013WR014410.
Cuthbert, M. O., and R. Mackay (2013), Impacts of nonuniform flow on estimates of vertical streambed flux, *Water Resour. Res.*, *49*, 19–28, doi:10.1029/2011WR011587.
Daniluk, T. L., L. K. Lautz, R. P. Gordon, and T. A. Endreny (2013), Surface water-groundwater interaction at restored streams and associated reference reaches, *Hydrol. Processes*, *27*(25), 3730–3746, doi:10.1002/hyp.9501.
De Doncker, L. (2010), A fundamental study on exchange processes in river ecosystems, PhD thesis, 475 pp., Universiteit Ghent, Ghent, Belgium.
Dujardin, J., C. Anibas, J. Bronders, P. Jamin, K. Hamonts, W. Dejonghe, S. Brouyere, and O. Batelaan (2014), Combining flux estimation techniques to improve characterization of groundwater-surface-water interaction in the Zenne River, Belgium, *Hydrogeol. J.*, *22*(7), 1657–1668, doi:10.1007/s10040-014-1159-4.
Engelhardt, I., M. Piepenbrink, N. Trauth, S. Stadler, C. Kludt, M. Schulz, C. Schuth, and T. A. Ternes (2011), Comparison of tracer methods to quantify hydrodynamic exchange within the hyporheic zone, *J. Hydrol.*, *400*(1–2), 255–266, doi:10.1016/j.jhydrol.2011.01.033.
Fritz, B. G., D. P. Mendoza, and T. J. Gilmore (2009), Development of an electronic seepage chamber for extended use in a river, *Ground Water*, *47*(1), 136–140, doi:10.1111/j.1745-6584.2008.00491.x.
Gordon, R. P., L. K. Lautz, M. A. Briggs, and J. M. McKenzie (2012), Automated calculation of vertical pore-water flux from field temperature time series using the VFLUX method and computer program, *J. Hydrol.*, *420*, 142–158, doi:10.1016/j.jhydrol.2011.11.053.
Goto, S., M. Yamano, and M. Kinoshita (2005), Thermal response of sediment with vertical fluid flow to periodic temperature variation at the surface, *J. Geophys. Res.*, *110*, B01106, doi:10.1029/2004JB003419.
Hatch, C. E., A. T. Fisher, J. S. Revenaugh, J. Constantz, and C. Ruehl (2006), Quantifying surface water-groundwater interactions using time series analysis of streambed thermal records: Method development, *Water Resour. Res.*, *42*, W10410, doi:10.1029/2005WR004787.
Hester, E. T., M. W. Doyle, and G. C. Poole (2009), The influence of in-stream structures on summer water temperatures via induced hyporheic exchange, *Limnol. Oceanogr.*, *54*(1), 355–367, doi:10.4319/lo.2009.54.1.0355.
Irvine, D. J., L. K. Lautz, M. A. Briggs, R. P. Gordon, and J. M. McKenzie (2015a), Experimental evaluation of the applicability of phase, amplitude, and combined methods to determine water flux and thermal diffusivity from temperature time series using VFLUX 2, *J. Hydrol.*, *531*, 728–737, doi:10.1016/j.jhydrol.2015.10.054.
Irvine, D. J., R. H. Cranswick, C. T. Simmons, M. A. Shanafield, and L. K. Lautz (2015b), The effect of streambed heterogeneity on groundwater-surface water exchange fluxes inferred from temperature time series, *Water Resour. Res.*, *51*, 198–212, doi:10.1002/2014WR015769.
Karan, S., P. Engesgaard, and J. Rasmussen (2014), Dynamic streambed fluxes during rainfall-runoff events, *Water Resour. Res.*, *50*, 2293–2311, doi:10.1002/2013WR014155.
Käser, D. H., A. Binley, and A. L. Heathwaite (2013), On the importance of considering channel microforms in groundwater models of hyporheic exchange, *River Res. Appl.*, *29*(4), 528–535, doi:10.1002/rra.1618.
Keery, J., A. Binley, N. Crook, and J. W. N. Smith (2007), Temporal and spatial variability of groundwater-surface water fluxes: Development and application of an analytical method using temperature time series, *J. Hydrol.*, *336*(1–2), 1–16, doi:10.1016/j.jhydrol.2006.12.003.
Krause, S., L. Heathwaite, A. Binley, and P. Keenan (2009), Nitrate concentration changes at the groundwater-surface water interface of a small Cumbrian river, *Hydrol. Processes*, *23*(15), 2195–2211, doi:10.1002/hyp.7213.
Krause, S., T. Blume, and N. J. Cassidy (2012), Investigating patterns and controls of groundwater up-welling in a lowland river by combining Fibre-optic Distributed Temperature Sensing with observations of vertical hydraulic gradients, *Hydrol. Earth Syst. Sci.*, *16*(6), 1775–1792, doi:10.5194/hess-16-1775-2012.
Langston, G., M. Hayashi, and J. W. Roy (2013), Quantifying groundwater-surface water interactions in a proglacial moraine using heat and solute tracers, *Water Resour. Res.*, *49*, 5411–5426, doi:10.1002/wrcr.20372.
Lapham, W. W. (1989), Use of temperature profiles beneath streams to determine rates of vertical ground-water flow and vertical hydraulic conductivity, *Water Supply Pap. 2337*, 44 pp., U.S. Geol. Surv., Denver, Colo.
Lautz, L. K. (2010), Impacts of nonideal field conditions on vertical water velocity estimates from streambed temperature time series, *Water Resour. Res.*, *46*, W01509, doi:10.1029/2009WR007917.
Lewandowski, J., L. Angermann, G. Nutzmann, and J. H. Fleckenstein (2011), A heat pulse technique for the determination of small-scale flow directions and flow velocities in the streambed of sand-bed streams, *Hydrol. Processes*, *25*(20), 3244–3255, doi:10.1002/hyp.8062.
Li, X., G. Bi, S. Stankovic, and A. M. Zoubir (2011), Local polynomial Fourier transform: A review on recent developments and applications, *Signal Process.*, *91*(6), 1370–1393, doi:10.1016/j.sigpro.2010.09.003.
Luce, C. H., D. Tonina, F. Gariglio, and R. Applebee (2013), Solutions for the diurnally forced advection-diffusion equation to estimate bulk fluid velocity and diffusivity in streambeds from temperature time series, *Water Resour. Res.*, *49*, 488–506, doi:10.1029/2012WR012380.
McCallum, A. M., M. S. Andersen, G. C. Rau, and R. I. Acworth (2012), A 1-D analytical method for estimating surface water-groundwater interactions and effective thermal diffusivity using temperature time series, *Water Resour. Res.*, *48*, W11532, doi:10.1029/2012WR012007.
Menichino, G. T., and E. T. Hester (2014), Hydraulic and thermal effects of in-stream structure-induced hyporheic exchange across a range of hydraulic conductivities, *Water Resour. Res.*, *50*, 4643–4661, doi:10.1002/2013WR014758.
Noorduijn, S. L., M. Shanafield, M. A. Trigg, G. A. Harrington, P. G. Cook, and L. Peeters (2014), Estimating seepage flux from ephemeral stream channels using surface water and groundwater level data, *Water Resour. Res.*, *50*, 1474–1489, doi:10.1002/2012WR013424.
Nützmann, G., C. Levers, and J. Lewandowski (2014), Coupled groundwater flow and heat transport simulation for estimating transient aquifer-stream exchange at the lowland River Spree (Germany), *Hydrol. Processes*, *28*(13), 4078–4090, doi:10.1002/hyp.9932.
Pintelon, R., J. Schoukens, G. Vandersteen, and K. Barbe (2010a), Estimation of nonparametric noise and FRF models for multivariable systems-Part I: Theory, *Mech. Syst. Signal Process.*, *24*(3), 573–595, doi:10.1016/j.ymssp.2009.08.009.
Pintelon, R., J. Schoukens, G. Vandersteen, and K. Barbe (2010b), Estimation of nonparametric noise and FRF models for multivariable systems-Part II: Extensions, applications, *Mech. Syst. Signal Process.*, *24*(3), 596–616, doi:10.1016/j.ymssp.2009.08.010.
Rau, G. C., M. S. Andersen, A. M. McCallum, H. Roshan, and R. I. Acworth (2014), Heat as a tracer to quantify water flow in near-surface sediments, *Earth Sci. Rev.*, *129*, 40–58, doi:10.1016/j.earscirev.2013.10.015.

Rau, G. C., M. O. Cuthbert, A. M. McCallum, L. J. S. Halloran, and M. S. Andersen (2015), Assessing the accuracy of 1-D analytical heat tracing for estimating near-surface sediment thermal diffusivity and water flux under transient conditions, *J. Geophys. Res.*, *120*, 1551–1573, doi:10.1002/2015JF003466.

Riml, J., and A. Wörman (2015), Spatiotemporal decomposition of solute dispersion in watersheds, *Water Resour. Res.*, *51*, 2377–2392, doi:10.1002/2014WR016385.

Rosenberry, D. O. (2008), A seepage meter designed for use in flowing water, *J. Hydrol.*, *359*(1–2), 118–130, doi:10.1016/j.jhydrol.2008.06.029.

Roshan, H., G. C. Rau, M. S. Andersen, and I. R. Acworth (2012), Use of heat as tracer to quantify vertical streambed flow in a two-dimensional flow field, *Water Resour. Res.*, *48*, W10508, doi:10.1029/2012WR011918.

Schmadel, N. M., B. T. Neilson, and T. Kasahara (2014), Deducing the spatial variability of exchange within a longitudinal channel water balance, *Hydrol. Processes*, *28*(7), 3088–3103, doi:10.1002/hyp.9854.

Schmidt, C., O. Buttner, A. Musolff, and J. H. Fleckenstein (2014), A method for automated, daily, temperature-based vertical streambed water-fluxes, *Fund. Appl. Limnol.*, *184*(3), 173–181, doi:10.1127/1863-9135/2014/0548.

Schornberg, C., C. Schmidt, E. Kalbus, and J. H. Fleckenstein (2010), Simulating the effects of geologic heterogeneity and transient boundary conditions on streambed temperatures—Implications for temperature-based water flux calculations, *Adv. Water Resour.*, *33*(11), 1309–1319, doi:10.1016/j.advwatres.2010.04.007.

Selker, J. S., N. van de Giesen, M. Westhoff, W. Luxemburg, and M. B. Parlange (2006), Fiber optics opens window on stream dynamics, *Geophys. Res. Lett.*, *33*, L24401, doi:10.1029/2006GL027979.

Shanafield, M., G. Pohll, and R. Susfalk (2010), Use of heat-based vertical fluxes to approximate total flux in simple channels, *Water Resour. Res.*, *46*, W03508, doi:10.1029/2009WR007956.

Shanafield, M., C. Hatch, and G. Pohll (2011), Uncertainty in thermal time series analysis estimates of streambed water flux, *Water Resour. Res.*, *47*, W03504, doi:10.1029/2010WR009574.

Soto-Lopez, C. D., T. Meixner, and T. P. A. Ferre (2011), Effects of measurement resolution on the analysis of temperature time series for stream-aquifer flux estimation., *Water Resour. Res.*, *47*, W12602, doi:10.1029/2011WR010834.

Stallman, R. W. (1965), Steady one-dimensional fluid flow in a semi-infinite porous medium with sinusoidal surface temperature, *J. Geophys. Res.*, *70*(12), 2821–2827.

Striegl, A. M., and S. P. Loheide, 2nd (2012), Heated distributed temperature sensing for field scale soil moisture monitoring, *Ground Water*, *50*(3), 340–347, doi:10.1111/j.1745-6584.2012.00928.x.

van Berkel, M., G. Vandersteen, E. Geerardyn, R. Pintelon, H. J. Zwart, and M. R. de Baar (2014a), Frequency domain sample maximum likelihood estimation for spatially dependent parameter estimation in PDEs, *Automatica*, *50*(8), 2113–2119, doi:10.1016/j.automatica.2014.05.027.

van Berkel, M., H. J. Zwart, N. Tamura, G. M. D. Hogeweij, S. Inagaki, M. R. de Baar, and K. Ida (2014b), Explicit approximations to estimate the perturbative diffusivity in the presence of convectivity and damping. I. Semi-infinite slab approximations, *Phys. Plasmas*, *21*, 112507, doi:10.1063/1.4901309.

Vandersteen, G., U. Schneidewind, C. Anibas, C. Schmidt, P. Seuntjens, and O. Batelaan (2015), Determining groundwater-surface water exchange from temperature-time series: Combining a local polynomial method with a maximum likelihood estimator, *Water Resour. Res.*, *51*, 922–939, doi:10.1002/2014WR015994.

Vogt, T., P. Schneider, L. Hahn-Woernle, and O. A. Cirpka (2010), Estimation of seepage rates in a losing stream by means of fiber-optic high-resolution vertical temperature profiling, *J. Hydrol.*, *380*(1–2), 154–164, doi:10.1016/j.jhydrol.2009.10.033.

Wörman, A., J. Riml, N. Schmadel, B. T. Neilson, A. Bottacin-Busolin, and J. E. Heavilin (2012), Spectral scaling of heat fluxes in streambed sediments, *Geophys. Res. Lett.*, *39*, L23402, doi:10.1029/2012GL053922.